Journal of Energy and Natural Resources
2024, Vol. 13, No. 2, pp. 59-68
https://doi.org/10.11648/j.jenr.20241302.12

Research Article

Revealing the Mechanism of O_2 and Pressure Effects on the Corrosion of X80 Carbon Steel Under Supercritical CO_2 Conditions

Guanbin Liu, Shuai Wang, Tian Xue, Yu Liu*

School of Energy and Power Engineering, Dalian University of Technology, Dalian, China

Abstract

Pipeline transportation is widely used due to its ability to improve the efficiency of CO_2 transportation in Carbon Capture, Utilization, and Storage (CCUS). Within the transport pipelines, CO_2 fluid exists in a supercritical state and often contains various impurity gases such as O_2 and H_2O, which can easily cause steel corrosion, affecting the safety of pipeline operations. In this investigation, we examine the corrosion behavior of X80 carbon steel within a water-saturated supercritical CO_2 environment utilizing weight loss experiments, electrochemical tests, and surface analysis techniques. Furthermore, we explore the impact of pressure and oxygen on the corrosion process of X80 steel. The results indicated that X80 steel underwent severe corrosion under the experimental conditions, with $FeCO_3$ as the primary corrosion product. Both the introduction of oxygen and an increase in pressure accelerated the steel's corrosion, and the addition of oxygen led to the formation of a new corrosion product, Fe_2O_3. Electrochemical test results showed that changes in pressure did not significantly alter the electrochemical corrosion characteristics of the steel, but the introduction of oxygen decreased the electrochemical reaction resistance of X80 steel. Combined with surface analysis, the following conclusions were drawn: In a 50 ℃ supercritical CO_2 environment, the anode reaction of X80 steel corrosion is the active dissolution of iron, while the cathode reaction involves the dissolution and ionization of CO_2. Changes in pressure do not alter the corrosion mechanism, but the introduction of oxygen leads to oxygen corrosion reactions in the system, accelerating the anode reaction rate and thus increasing the degree of corrosion.

Keywords

CCUS, Pipeline Transportation, Supercritical CO_2, Steel Corrosion, Influence Mechanism

1. Introduction

With the continuous progress of social science and technology, the demand for energy from humans continues to grow, especially with the increasing consumption of fossil fuels, leading to large amounts of CO_2 emissions into the atmosphere [1]. This has caused serious consequences such as global warming, severely impacting the Earth's ecological environment. If the CO_2 content in the atmosphere is not strictly controlled, the greenhouse effect will become increasingly prominent, causing a series of environmental and ecological problems and limiting the sustainable development of human society [2]. CCUS technology is considered a promising technology for achieving large-scale carbon emis-

*Corresponding author: liuyu@dlut.edu.cn (Yu Liu)

Received: 24 April 2024; **Accepted:** 4 June 2024; **Published:** 13 June 2024

sions reduction and utilization from fossil fuels [3]. It is an important means for reducing CO_2 emissions and achieving sustainable development worldwide in the future. CCUS technology is currently able to significantly reduce CO_2 emissions from industrial production by transforming old processes. These factors indicate that carbon capture can be the first choice for reducing CO_2 levels in the atmosphere in the future, with tremendous development potential.

CCUS mainly includes capture, transport, utilization, and storage. With the introduction of the "dual-carbon" goal and the continuous implementation of various carbon reduction policies, CCUS is rapidly developing in China. However, issues such as technical implementation and safe operation still need to be addressed. Pipeline transport can achieve long-distance, large-scale CO_2 delivery, making it the most economical and environmentally friendly choice in CCUS transportation [4]. In pipeline transport, CO_2 is generally compressed into a supercritical state (sc_CO_2) [5]. However, due to the complex fluid phase inside the pipeline and the presence of a large amount of impurity gases, corrosion is likely to occur in the pipeline, restricting its safe operation. Due to the long-distance pipeline transport, changes in the phase of the transported fluid are likely to occur, and impurities such as O_2 may exist in the fluid, causing serious corrosion to pipeline materials. These issues urgently require in-depth research into the corrosion behavior of pipeline materials in sc_CO_2-O_2 environments to make better anti-corrosion decisions.

In recent years, a large number of researchers have conducted extensive studies on the corrosion behavior and mechanisms of pipeline materials in sc_CO_2 environments, achieving certain progress. Some researchers believe that pressure does not change the corrosion mechanism of pipeline steel subjected to CO_2 corrosion but only affects the corrosion process of the steel [6]. However, there is considerable controversy among researchers regarding the impact of O_2 on steel corrosion. Some researchers argue that O_2 can exacerbate the corrosion of steel in sc_CO_2 because of its strong oxidizing nature, which can oxidize Fe^{2+} to Fe^{3+}, thereby disrupting the formation of protective corrosion product film $FeCO_3$ and promoting cathodic reactions within the system. However, other scholars believe that O_2 can inhibit steel corrosion because cathodic oxygen reduction can generate a large amount of OH^-, leading to the formation of a protective corrosion product film on the steel substrate, thus entering the passivation zone and inhibiting further corrosion of the steel. Currently, due to the difficulty of conducting electrochemical tests in sc_CO_2 environments, research on CO_2 corrosion of pipeline steel mainly focuses on mass loss and surface characterization. To fundamentally reveal the corrosion behavior and mechanism of pipeline steel in sc_CO_2, in-situ electrochemical tests are needed to track the evolution of steel surface corrosion processes and determine the impact of factors such as pressure and O_2.

In conclusion, the current research on steel corrosion in sc_CO_2 environments is not comprehensive enough, especially regarding the disputed influence of O_2 on corrosion. Therefore, it is necessary to study the corrosion characteristics and mechanisms of supercritical CO_2 transportation pipelines under different pressures and oxygen concentrations. By employing methods such as high-temperature and high-pressure reaction vessels, surface characterization techniques, and electrochemical tests, a thorough investigation into the effects of pressure and oxygen content on steel corrosion behavior and mechanisms in sc_CO_2 environments can be conducted. The research results can provide theoretical support for the safe operation of CO_2 transportation processes.

2. Experimental

2.1. Material and Solution

This study utilized X80 carbon steel, which was fabricated into rectangular specimens measuring 40×10×3mm ^{3}for corrosion weight loss experiments and surface characterization. The effective area was 7.23cm ^{2}. For electrochemical tests, working electrode dimensions were circular samples of Φ12×3mm ^{2}, with an effective area of 0.25cm ^{2}. The chemical composition is shown in Table 1.

Table 1. *Composition of X80 carbon steel (Mass score%).*

C	Si	Mn	S	Cr	Cu	Fe
0.046	0.30	1.76	0.0014	0.023	0.22	Balance

2.2. Corrosion Electrochemistry Experiment

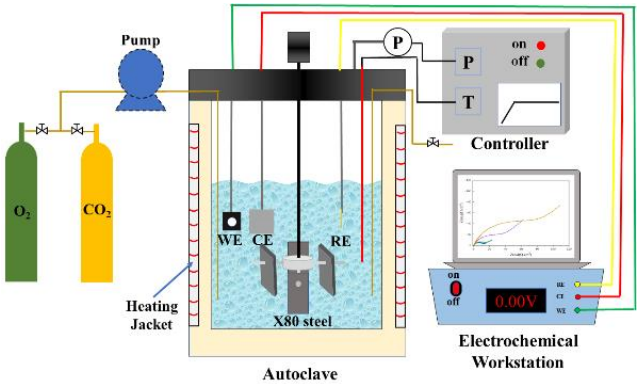

Figure 1. *Schematic of the sc_CO_2 autoclave testing setup.*

All experiments were conducted in a high-temperature and high-pressure reaction vessel as shown in Figure 1, where X80 carbon steel served as the working electrode, Pt foil as the counter electrode, and Pt wire as the reference electrode,

forming the three-electrode system for electrochemical testing. Additionally, within the reaction vessel, there was a polytetrafluoroethylene sample holder used for corrosion weight loss experiments and surface characterization. Specific test parameters for sc_CO_2 saturated water with/without O_2 (including temperature, pressure, oxygen content, time, etc.) are detailed in Table 2.

Table 2. *Test conditions.*

T (℃)	P (MPa)	O_2	Time (h)
50	8	0	132
	8	2%	
	10	0	
	10	2%	

The solution was pre-saturated with high-purity CO_2. fter loading the samples and electrodes into the reaction vessel, the pre-treated solution was added, and the reaction vessel was quickly sealed. Subsequently, CO_2 was purged again, deoxygenating for over 2 hours. The reaction vessel was then heated to the experimental temperature, followed by injecting gases to reach the experimental pressure. Electrochemical tests were conducted, including open circuit potential (OCP), linear polarization resistance (LPR), electrochemical impedance spectroscopy (EIS), and potentiodynamic polarization (PC) scans [7]. LPR testing included a potential range of ±10mV vs OCP and a scan rate of 0.125mV/s. EIS testing involved a frequency range of 0.01Hz to 1MHz with an AC amplitude of 10mV vs OCP. PC testing had a scan rate of 1mV/s and a scan range of ±250mV vs OCP [8].

2.3. Mass Loss Tests and Surface Characterization

After the designated corrosion time, the corroded samples were removed from the reaction vessel, with three used for calculating the corrosion rate and one used for surface characterization of corrosion products. Carlk solution was used to remove the corrosion products for measuring the mass loss before and after corrosion. Carlk solution was used to remove the corrosion products for measuring the mass loss before and after corrosion. Therefore, the corrosion rate (mm/y) of the steel samples can be calculated as follows [9]:

$$CR = (87600 \times \Delta m)/\rho A t \quad (1)$$

where CR icorresponds to the corrosion rate (mm/y), Δm (g) is the mass loss of the sample before corrosion test and after descaling corrosion priducts; ρ irepresents the density of the sample (g/cm^3), A the surface area of the sample (mm^2), and t the corrosion time (h).

The surface morphology of the corrosion products was observed using scanning electron microscopy (SEM), and the elemental composition of the corrosion products was analyzed using energy-dispersive spectroscopy (EDS). Additionally, X-ray diffraction (XRD) was employed to identify the phase composition of the corrosion products.

3. Results and Discussion

3.1. Mass Loss Measurement

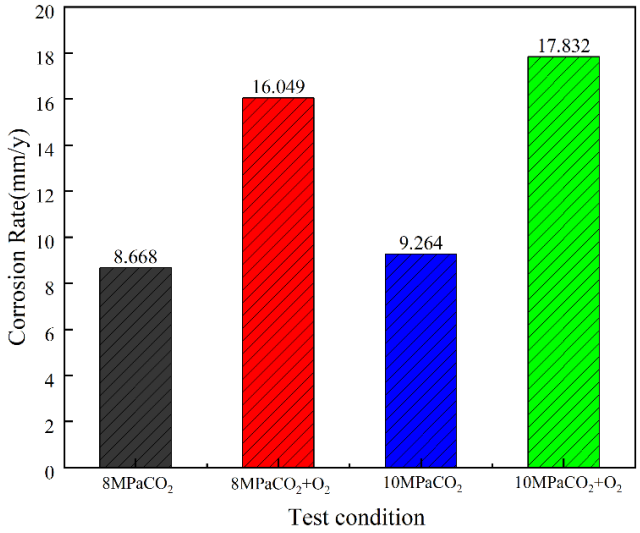

Figure 2. *The general corrosion rate of X80 steel in different environments.*

Figure 2 shows the weight loss corrosion rates of samples under different experimental conditions. It can be seen from Figure 2 that X80 steel experienced severe corrosion, with a high corrosion rate. At a temperature of 50 ℃, the corrosion rate was 8.668 mm/y when the injection pressure of CO_2 was 8 MPa. With the introduction of 2% O_2 into 8 MPa CO_2, the corrosion rate increased to 16.049 mm/y. When injecting 10 MPa CO_2, the corrosion rate was 9.264 mm/y, and with 2% O_2 in 10 MPa CO_2, the corrosion rate reached 17.832 mm/y. It can be observed that in 50 ℃ sc_CO_2, increasing the pressure from 8 MPa to 10 MPa typically leads to an increase in the corrosion rate of the steel. Additionally, in all oxygen-free systems, the corrosion rate is half that of oxygen-containing systems. The presence of O_2 in the system significantly increases the corrosion rate, consistent with previous research results [10]. Increasing pressure directly alters the solubility of gases in the system, leading to more corrosive gases such as CO_2 dissolving into the water, increasing the concentration of substances involved in the corrosion reaction, thereby accelerating the reaction process. O_2 acts as a strong oxidant, accelerating the oxidation reaction

on the surface of steel and speeding up the corrosion process. Therefore, with the increase in pressure or O_2 content in sc_CO_2, the average corrosion rate of X80 steel gradually increases, and the promoting effect of O_2 on the corrosion rate is more pronounced than increasing pressure.

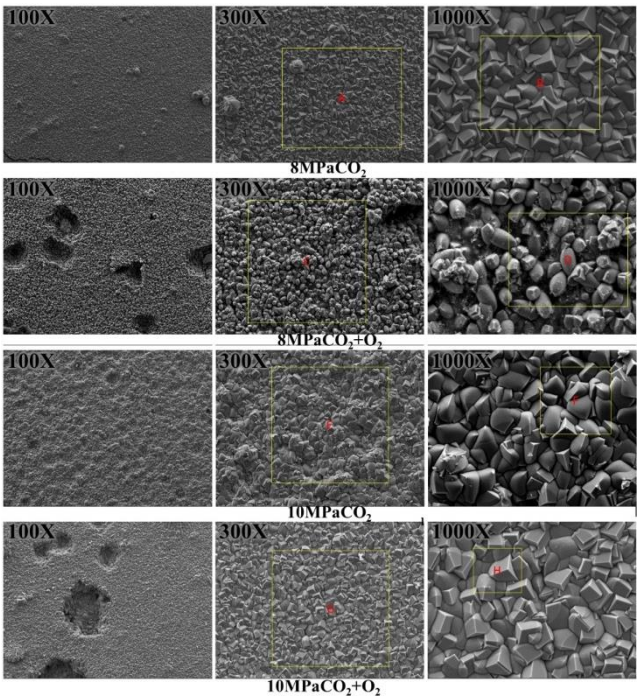

Figure 3. *SEM morphology of X80 steel in different environments.*

3.2. SEM, EDS and XRD Analysis

Figure 3 depicts the morphology of corrosion products formed on the surface of X80 steel after a 132-hour sc_CO_2 corrosion test, showing a significant amount of corrosion products uniformly adhered to the steel surface. In an 8 MPa environment, the corrosion product film consists of a large amount of grain corrosion products, and the formed corrosion product film is dense with a uniform distribution, effectively protecting the substrate from further corrosion. When the pressure increases to 10 MPa, the corrosion product film undergoes noticeable changes, with slightly larger grain sizes on the film surface and an uneven distribution of accumulation. However, the corrosion products still tightly adhere and provide protection to the substrate. In the 8 MPa sc_CO_2-O_2 environment, the corrosion product film changes, with corrosion products evenly distributed on the steel surface but the film layer showing obvious defects, possibly due to localized corrosion. At the same time, there is a significant change in the grain size of the corrosion products, a loose structure, and a larger porosity, resulting in a weakened protective effect of the corrosion product film on the substrate. When the pressure in the O_2-containing system increases to 10 MPa, defects from localized corrosion still exist on the steel surface, with larger corrosion product grains densely and evenly distributed on the substrate surface.

Table 3 presents the EDS test results of X80 steel in different corrosion environments, with the test areas marked in Figure 2. It can be seen that all the corrosion products on the sample surfaces are composed of C, O, Fe, and Mn elements, with a relatively low Mn content, possibly from the X80 carbon steel substrate, and can be ignored. In the sc_CO_2 system without oxygen, the EDS results show a higher atomic percentage of O elements compared to the O_2-containing system, suggesting that the main corrosion product is $FeCO_3$. In the O_2-containing system, based on the atomic composition of Fe, C, and O elements, it is inferred that besides $FeCO_3$, other iron oxides are also present in the corrosion products, which requires further analysis in conjunction with XRD test results.

Table 3. *The results of scales EDS analyzing (atom fraction, %).*

Location	C	O	Fe	Mn	Location	C	O	Fe	Mn
A	16.87	62.27	20.25	0.61	E	18.39	61.78	19.51	0.32
B	17.95	59.55	21.88	0.62	F	17.84	62.03	19.86	0.27
C	28.59	48.47	21.52	1.43	G	28.56	50.25	20.18	1.01
D	28.90	47.94	21.68	1.48	H	28.33	49.98	20.69	1.01

Figure 4 shows the XRD test results of X80 steel in different corrosion environments. From the analysis results, it is evident that in the sc_CO_2 system, the corrosion product film is mainly composed of $FeCO_3$, which is consistent with the EDS analysis results [11]. In the sc_CO_2-O_2 system, the presence of O_2 leads to the appearance of new Fe_2O_3 corrosion products.

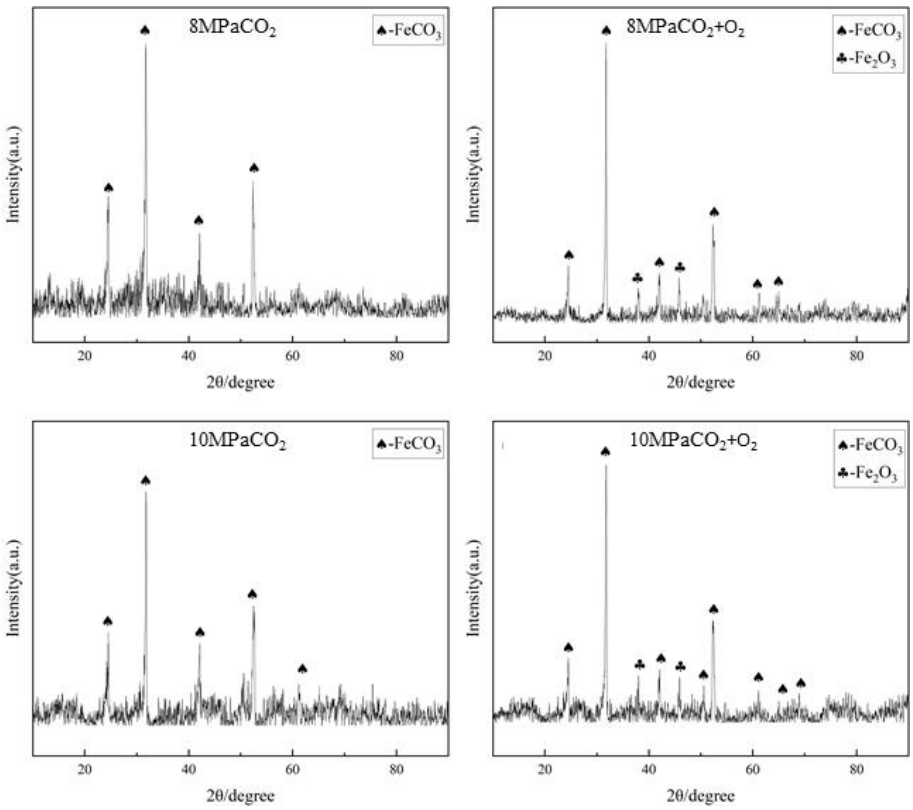

Figure 4. *XRD results of corrosion of X80 steel in different supercritical environments.*

Combining the SEM, EDS, and XRD results, it can be concluded that in the sc_CO_2 environment, the corrosion products are mainly composed of $FeCO_3$, forming a dense and uniform corrosion product film that effectively protects the substrate from further corrosion. With the increase in system pressure, there are no significant changes in the corrosion products on the surface of X80 steel and the structure of the formed film layer, indicating that increasing pressure does not change its corrosion mechanism but only accelerates the corrosion reaction rate, leading to more severe corrosion. In the sc_CO_2-O_2 environment, the corrosion products are $FeCO_3$ and Fe_2O_3, and due to the presence of O_2, there is a significant change in the corrosion product film structure, with a loose distribution of corrosion products, an increase in porosity of the film layer on the substrate surface, weakening the protective effect on the substrate, thus causing a greater corrosion rate. This indicates that an increase in O_2 content in the system directly changes the corrosion behavior of X80 steel, leading to the formation of new corrosion products and also affecting the morphology and type of corrosion products [12]. This weakens the protective role of the corrosion product layer on the substrate, thereby accelerating the corrosion process.

3.3. OCP and LPR Analysis

Figure 5 shows the relationship between the open circuit potential (OCP) of X80 steel in different sc_CO_2 environments over time. It can be observed that there is a significant difference in OCP among different systems, and all OCP values continuously shift positively over time, indicating that as corrosion reactions occur, the reaction rate within the system gradually slows down. In the initial stage of corrosion reaction, OCP changes most rapidly, indicating the most active corrosion reactions within the system. In the mid-reaction stage, OCP begins to stabilize and increase, indicating stable corrosion reactions within the system.

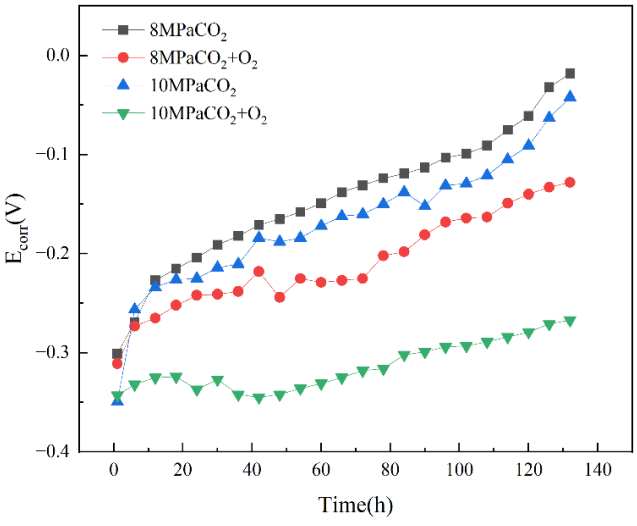

Figure 5. *The relationship between the OCP and time for X80 steel under various sc_CO_2 environmental conditions.*

In the final stage of corrosion, OCP approaches 0 V, indicating the formation of a stable corrosion product layer on the metal surface, hindering further corrosion reactions. In the 8 MPa environment, OCP is most positive, corresponding to the weakest corrosion tendency. As pressure increasing, OCP shows a slight negative shift, indicating a slightly stronger corrosion tendency within the system. When O_2 is introduced, OCP shows a significant negative shift, enhancing the corrosion tendency within the system and thus accelerating the corrosion rate.

Table 4 shows the relationship between the linear polarization resistance (R_p) of X80 steel obtained from fitting LPR results under different experimental conditions and time. From Table 4, it can be observed that in all experimental conditions, R_p is minimal in the initial stage of the reaction, corresponding to the minimum electrochemical reaction resistance and the fastest corrosion reaction rate. In the mid-reaction stage, R_p stabilizes and increases within a small range, indicating stable corrosion reactions. In the late reaction stage, R_p rapidly increases, indicating an increase in corrosion reaction resistance and the minimum corrosion rate. The Rp value is highest in the 8 MPa environment and lowest in the 10 MPa sc_CO_2-O_2 environment, which is consistent with the OCP change pattern.

Table 4. *The relationship between the R_p and time for X80 steel under various supercritical CO_2 environmental conditions.*

Time (h)	8 MPaCO_2 R_p ($\Omega.cm^2$)	8 MPaCO_2-O_2 R_p ($\Omega.cm^2$)	10 MPaCO_2 R_p ($\Omega.cm^2$)	10 MPaCO_2-O_2 R_p ($\Omega.cm^2$)
1	12.823	12.673	12.52	13.037
24	25.075	20.897	18.165	16.759
48	28.923	24.186	19.113	15.242
72	30.727	27.588	22.975	18.012
96	93.414	64.706	65.077	21.241
132	186.201	124.611	141.5	30.948

An increase in pressure and the addition of O_2 will change the electrochemical behavior of the system, manifested as more negative OCP and smaller R_p, promoting the occurrence of corrosion reactions within the system. Moreover, the impact of O_2 on electrochemical behavior is greater than that of pressure; when O_2 is introduced while increasing system pressure, the degree of change in the system's electrochemical behavior is maximal.

3.4. PC and EIS Analysis

Figure 6 shows the polarization curves of X80 steel obtained under all experimental conditions, and the relevant parameters fitted by Tafel are shown in Table 5. It can be observed that the polarization curves experience different degrees of shift due to the influence of pressure and oxygen, but the overall shape remains unchanged, and there is no passivation phenomenon. Regardless of the presence of O_2, both cathodic and anodic processes are mainly controlled by activation, with the corrosion reaction being more influenced by the cathodic reaction [13]. When the pressure inside the system is increased, the anodic current density decreases while the cathodic current density increases, resulting in a negative shift in corrosion potential and an increase in corrosion current density. In the sc_CO_2 environment, increasing pressure can enhance the solubility of CO_2 in the system, leading to an increase in acidity within the system and accelerating the corrosion process. When a small amount of O_2 is introduced, the cathodic current density further increases, while the anodic current density decreases further, resulting in a more negative corrosion potential and a higher corrosion current density. Fe^{2+} can be oxidized to Fe^{3+} by O_2, leading to a significant increase in cathodic current density in the presence of O_2. O_2 can combine with H^+ to generate additional oxygen corrosion reactions, thereby accelerating the corrosion reaction rate in the system.

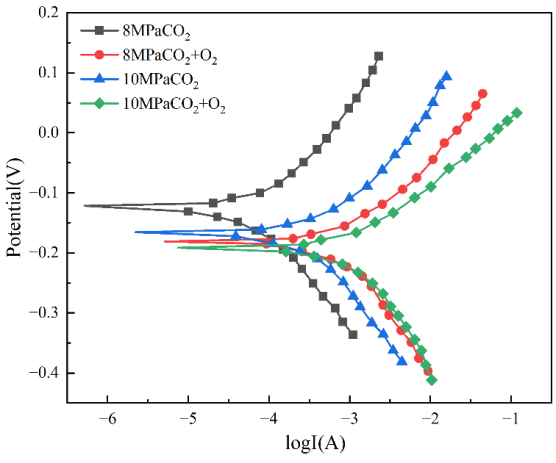

Figure 6. *The polarization curves of X80 steel after 132 hours of corrosion in different environments.*

Table 5. *Parameters of the polarization curves for X80 steel after 132 hours of corrosion in different environments.*

Conditions	Ecorr (V)	Icorr (A/cm^2)	ba (mV/dec)	bc (mV/dec)
8 MPaCO_2	-0.12151	0.01499	0.18554	-0.13665
8 MPaCO_2-O_2	-0.18093	0.04445	0.14991	-0.17689
10 MPaCO_2	-0.16546	0.03499	0.16935	-0.1629
10 MPaCO_2-O_2	-0.19121	0.05377	0.10962	-0.22591

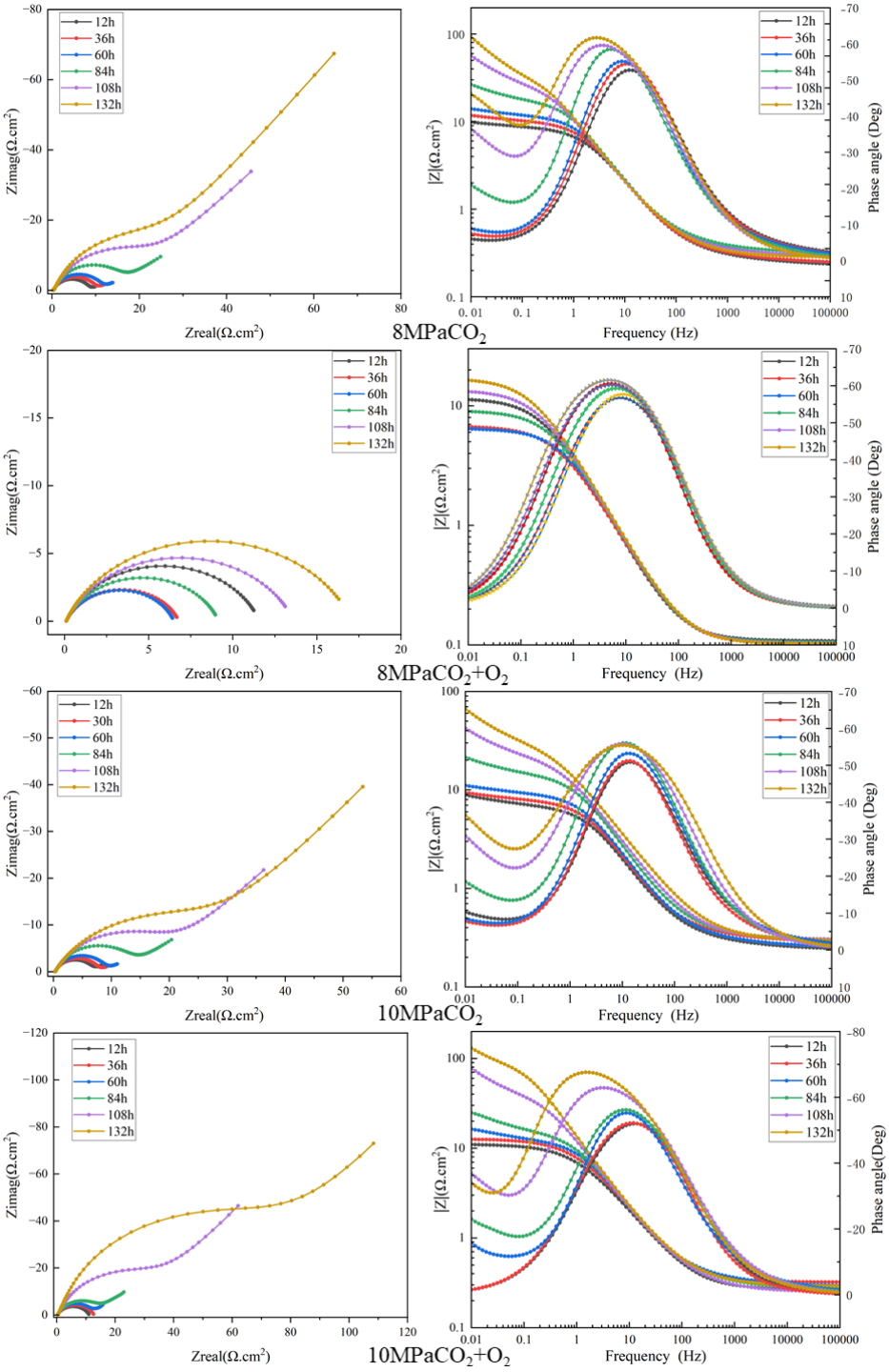

Figure 7. *EIS plots of X80 steel at different moments in different environments.*

Figure 7 shows the EIS results obtained for X80 steel under different environments. It can be seen that the impedance spectrum exhibits a capacitive semicircle in the high-frequency region and a diffusion impedance in the low-frequency region. The impedance gradually increases as the reaction progresses, manifested by the increasing radius of the capacitive arc and the growing diffusion impedance. In an sc_CO_2 environment without O_2, increasing pressure causes the capacitive arc in the high-frequency region to shrink and the diffusion impedance to decrease, indicating a certain degree of enhancement in corrosion. Particularly in the 8 MPa sc_CO_2-O_2 environment, due to the influence of O_2, the diffusion impedance in the low-frequency region disappears, and the impedance graph shows only a high-frequency capacitive arc, which initially contracts and then expands. When the pressure in the O_2-containing system is increased to 10 MPa, in the early stages of corrosion, there is only a high-frequency capacitive arc in the impedance, which gradually transitions to diffusion impedance and becomes larger as the corrosion reaction progresses.

To better visually represent the corrosion resistance of X80 steel in different environments, the EIS data were fitted using an equivalent circuit in Figure 8, and Figure 9 provides specific fitting parameter results. It can be observed that when the pressure in the system increases, the impedance decreases, indicating that increasing the pressure promotes the corrosion process of the steel. When O_2 is introduced into the system, the impedance further decreases, indicating that the presence of O_2 significantly promotes the corrosion process of the steel, which is consistent with the results of mass loss experiments.

By comprehensively analyzing the time-varying characteristics of the alternating current impedance spectra of X80 steel in different environmental systems, the corrosion reaction of X80 steel in sc_CO_2 can be divided into three different stages. In the initial stage, the corrosion rate of exposed X80 carbon steel electrodes increase, which is due to the selective dissolution of ferrite, leaving a more corrosion-resistant intact iron carbide structure. Subsequently, this material induces galvanic coupling effects, increasing the area where cathodic reactions occur and forming a loose, porous layer. Finally, as the corrosion products accumulate continuously on the metal surface, they gradually fill the pores of the iron carbide layer and form a corrosion film that can significantly hinder the corrosion reaction, thus reducing the corrosion rate. An increase in pressure leads to the shrinkage of the high-frequency capacitive arc in the EIS, thereby reducing the electrochemical reaction resistance and promoting the corrosion process of X80 steel. However, changes in pressure do not result in new corrosion mechanisms in the system. After O_2 is introduced into the system, significant changes occur in the EIS, with the most significant change being the disappearance of the diffusion impedance in the low-frequency region during the initial stage of corrosion, indicating that O_2 affects the formation process of corrosion products on the metal surface.

In the initial stage of corrosion, when O_2 is absent from the system, the corrosion reaction mainly involves the dissolution of ferrite and hydrogen evolution reactions. When O_2 is present in the system, more ferrite dissolves from the metal surface, leading to a rapid increase in Fe^{2+} concentration.

The corrosion reaction continues, and in the absence of O_2 in the system, the anode continues to dissolve, leaving residual carburized areas on the steel surface, thereby creating pores. This provides favorable locations for the corrosion reaction, accelerating the corrosion process and increasing the corrosion rate. When the system contains oxygen, the originally unstable corrosion products undergo oxidation by oxygen, forming a stable iron oxide layer that hinders the diffusion of ions from the metal surface into the solution. In the later stages of the corrosion process, when there is no oxygen in the system, the corrosion reaction in the system still involves anodic metal dissolution. Corrosion product $FeCO_3$ begins to accumulate on the surface of the substrate, forming a protective film. In the sc_CO_2-O_2 system, due to continuous oxidation by O_2, the deposition rate of the oxidized corrosion product film on the surface increases rapidly, and the structure of the film gradually stabilizes, resulting in a more significant hindrance to the diffusion of ions and a stronger protective effect on pipeline materials.

In summary, the differences in corrosion electrochemical behavior of X80 steel under the influence of O_2 primarily stem from the following factors: O_2 affects the cathodic reaction process in the initial stage, introducing an oxygen corrosion process, thereby oxidizing the unstable sub-iron oxide generated in the corrosion intermediate reaction into a less easily decomposable iron oxide, which can effectively deposit on the metal surface, hinder the diffusion of substances, promote the formation of more protective $FeCO_3$ corrosion product film.

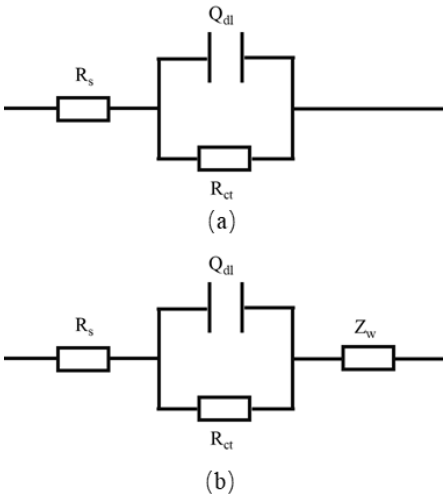

Figure 8. *EIS fitting equivalent circuits (a) 8 MPa CO_2+O_2 (at all time), 10 MPa CO_2+O_2 (at 12h and 36h); (b) remaining EIS. (R_s is the resistance of solution; Q_{dl} is constant phase element (CPE) representing the double-charge layer capacitance; R_{ct} is charge transfer resistance; Z_w is diffusion impedance).*

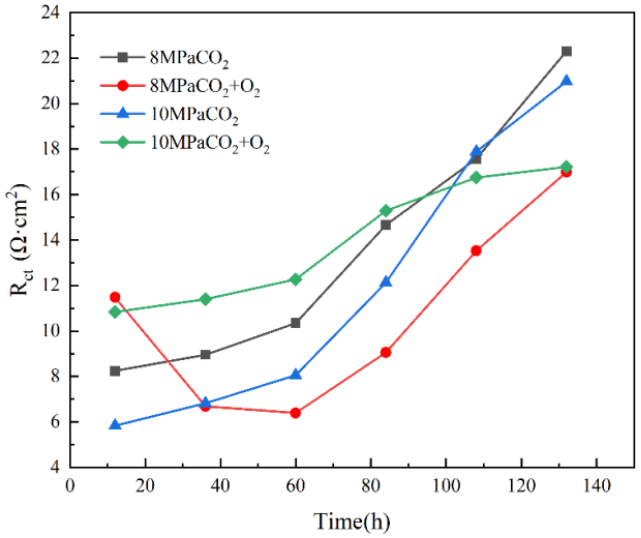

Figure 9. *R_{ct} of X80 steel at different times in different environments.*

4. Conclusions

Corrosion weight loss results indicate that increasing pressure and adding O_2 increase the corrosion rate of X80 steel, with O_2 having a more pronounced effect on accelerating corrosion rates.

Surface analysis results show that the corrosion product of X80 steel in the sc_CO_2 system is mainly $FeCO_3$, and the addition of O_2 results in the formation of a new corrosion product, Fe_2O_3.

Electrochemical measurements reveal that increasing pressure does not change the corrosion mechanism of X80 steel, while the addition of O_2 leads to oxygen corrosion reactions and affects the cathodic reaction process, oxidizing the easily decomposable intermediate corrosion products into a stable corrosion product layer, promoting the formation of protective $FeCO_3$ corrosion products.

This study only focuses on certain environmental factors, as there are numerous factors influencing CO_2 corrosion, such as material composition [14], exposure duration [15], moisture content [16], as well as the presence of impurity gases like SO_2 and NO_2 [17]. Therefore, future research is recommended to comprehensively consider all these factors to derive more comprehensive conclusions.

Abbreviations

CCUS	Carbon Capture, Utilization, and Storage
sc_CO_2	Supercritical CO_2
OCP	Open Circuit Potential
LPR	Linear Polarization Resistance
EIS	Electrochemical Impedance Spectroscopy
SEM	Scanning Electron Microscopy
EDS	Energy-Dispersive Spectroscopy
XRD	X-ray Diffraction

Acknowledgments

The authors thank the support of analytical and testing center of Dalian University of Technology.

Author Contributions

Guanbin Liu: Writing – original draft, Writing – review & editing, Data curation

Shuai Wang: Software, Validation

Tian Xue: Investigation, Software, Formal Analysis

Yu Liu: Writing – review & editing, Supervision, Methodology

Funding

This work is supported by the National Key Research and Development Program of China (Grant 2023YFB4104203), the National Natural Science Foundation of China (Grant U23B2090) and the Liaoning Provincial Science and Technology Plan Project (Science and Technology Research Special Project, Grant 2023JH1/ 10400003).

Data Availability Statement

The data is available from the corresponding author upon reasonable request.

Conflicts of Interest

All the authors do not have any possible conflicts of interest.

References

[1] El-Kady AH, Amin MT, Khan F, El-Halwagi MM. Analysis of CO_2 pipeline regulations from a safety perspective for offshore carbon capture, utilization, and storage (CCUS). Journal of Cleaner Production. 2024, 439, 140734. https://doi.org/10.1016/j.jclepro.2024.140734

[2] Zeng D, Dong B, Yu Z, Huang Z, Yi Y, Yu H. Design of water-based annulus protection fluid for CO_2 flooding injection well. Journal of Petroleum Science and Engineering. 2021, 205, 108726. https://doi.org/10.1016/j.petrol.2021.108726

[3] Nath F, Mahmood MN, Yousuf N. Recent advances in CCUS: A critical review on technologies, regulatory aspects and economics. Geoenergy Science and Engineering. 2024, 186, 212726. https://doi.org/10.1016/j.geoen.2024.212726

[4] Sun H, Wang H, Zeng Y, Liu J. Corrosion challenges in supercritical CO_2 transportation, storage, and utilization—a review. Renewable and Sustainable Energy Reviews. 2023, 179, 113292. https://doi.org/10.1016/j.rser.2023.113292

[5] Hua Y, Barker R, Neville A. The influence of SO_2 on the tolerable water content to avoid pipeline corrosion during the transportation of supercritical CO_2. International Journal of Greenhouse Gas Control. 2015, 37, 412-23. https://doi.org/10.1016/j.ijggc.2015.03.031

[6] Li YY, Jiang ZN, Zhang QH, Lei Y, Wang X, Zhang GA. Unveiling the influential mechanism of O_2 on the corrosion of N80 carbon steel under dynamic supercritical CO_2 conditions. Corrosion Science. 2022, 205, 110436. https://doi.org/10.1016/j.corsci.2022.110436

[7] Alberto da Silva C, Filho D, Pimentel T, Panossian Z. Analysis of crude oil effect for CO_2 corrosion of carbon steel - A rotating cylinder electrode approach. Geoenergy Science and Engineering. 2023, 229, 212085. https://doi.org/10.1016/j.geoen.2023.212085

[8] Wang W, Guang Y, Liu W, Shen K, Huffman M, Wang Q. Experimental investigation of stress corrosion on supercritical CO_2 transportation pipelines against leakage for CCUS applications. Energy Reports. 2023, 9, 266-76. https://doi.org/10.1016/j.egyr.2022.11.179

[9] Zhao S, Liao K, Wang X, Zhou F, Song X, He G. Corrosion behavior of 35CrMo steel in a CO_2/O_2 coexistent simulating environment of fire-drive tail gas. Materials Chemistry and Physics. 2021, 272, 125016. https://doi.org/10.1016/j.matchemphys.2021.125016

[10] He L, Zhang Q, Chen W, Wang Y, Wang M, Huang Y. Unraveling short-term O_2 contamination on under deposit corrosion of X65 pipeline steel in CO_2 saturated solution. Corrosion Science. 2024, 233, 112113. https://doi.org/10.1016/j.corsci.2024.112113

[11] Azevedo Rodrigues TRS, Marcolino JB, Moraes MK, Lopes NF, Costa EM. Influence of CO_2 subcritical and supercritical pressures on the protective properties of corrosion product scales formed on X65 steel. The Journal of Supercritical Fluids. 2024, 206, 106184. https://doi.org/10.1016/j.supflu.2024.106184

[12] Yu C, Liu Y, Chen J, Wang Z, Guo Q, Wu Y. Revealing the effect of O_2, SO_2 and H_2O in supercritical CO_2 on the corrosion behavior of 316 L steel at elevated temperature. Surfaces and Interfaces. 2024, 49, 104433. https://doi.org/10.1016/j.surfin.2024.104433

[13] Li C, Xiang Y, Wang R, Yuan J, Xu Y, Li W. Exploring the influence of flue gas impurities on the electrochemical corrosion mechanism of X80 steel in a supercritical CO_2-saturated aqueous environment. Corrosion Science. 2023, 211, 110899. https://doi.org/10.1016/j.corsci.2022.110899

[14] Zhou L, Huang X, Song W, Huang C, Liu H, Wang H. Multi-factor corrosion model of TP110TS steel in H_2S/CO_2 coexistence and life prediction of petroleum casings. International Journal of Pressure Vessels and Piping. 2024, 132, 105204. https://doi.org/10.1016/j.ijpvp.2024.105204

[15] Wang S, Wang S, Wen Z, Yao M, Wu M. Time-dependent high-pressure CO_2-induced corrosion and mechanical degradation in lightweight fly-ash cement/P110 steel system. Corrosion Science. 2024, 231, 111954. https://doi.org/10.1016/j.corsci.2024.111954

[16] Hong H, Ye T, Zhang J, Wang ZM. Corrosion mitigation behavior of mild steel in supercritical CO_2 environments with varying the solution volume. Corrosion Science. 2024, 229, 111853. https://doi.org/10.1016/j.corsci.2024.111853

[17] Liao K, Qin M, Yang N, He G, Zhao S, Zhang S. Corrosion main control factors and corrosion degree prediction charts in H_2S and CO_2 coexisting associated gas pipelines. Materials Chemistry and Physics. 2022, 292, 126838. https://doi.org/10.1016/j.matchemphys.2022.126838